Electronic Supplementary Material (ESI) for Lab on a Chip.


## Supporting Information

# Acoustophoretic focusing effects on particle synthesis and clogging in microreactors

Zhengya Dong[a], David Fernandez Rivas[b], Simon Kuhn[a,*]

[a]KU Leuven, Department of Chemical Engineering, Celestijnenlaan 200F, 3001 Leuven, Belgium

[b]Mesoscale Chemical Systems, MESA+ Institute, University of Twente, Enschede, The Netherlands

*simon.kuhn@kuleuven.be

## 1. Comparison of channel dimensions between reported and our developed microreactor

A quantitative comparison between reported and our developed reactor is provided in Table S1. Most of the acoustofluidic microfluidic devices reported in literature have focused on particle sorting and cell manipulation where a single straight channel is typically used. This approach results in small reactor volumes and low throughputs which makes it difficult to apply in realistic practical settings. Table S1 shows that a majority of reactors use a single straight channel with limited length (20-40 mm), and thus with volumes below 5 µL (the volume of our reactor is 20 times larger: 105 µL). The two examples with a channel volume of 25 µL and 127.5 µL rely on a large aspect ratio, i.e. a very large channel width compared to their depth. Such reactors are unsuitable for chemical synthesis as the mixing in the width direction will be poor due to the long diffusion distance. Having chemical synthesis in mind, an aspect ratio of 1 would be optimal, which is realized in our developed reactor. The technological advance of our work is that we have developed a numbered-up 'large scale' acoustofluidic chip for chemical synthesis, where five straight channels are connected in series, reaching a reactor volume of 105 µL and operating at flow rates up to 1.2 ml/min.

Table S1 Comparison of channel dimensions and chip layouts between reported reactors and the microreactor developed in this study.

| Reference | Channel dimensions (depth×width×length) ($mm^3$) | Channel volume (µL) | Chip layout | Application area |
|---|---|---|---|---|
| Neild *et al.* [1] | 0.2×5×25 | 25 | single straight channel | cell positioning |
| Fong *et al.* [2] | 0.2×0.9×40 | 0.72 | single straight channel | cell separation |
| Antfolk *et al.* [3] | 0.23×0.23×35 | 1.85 | single straight channel | enrichment of bacteria |
| Antfolk *et al.* [4] | 0.31×0.15×23 and 0.375×0.15×22 | 2.31 | single straight channel | tumor cell separation and enrichment |
| Gao *et al.* [5] | 0.284×0.252×25 | 1.79 | single straight channel | spatial manipulation of microparticles |
| Chen *et al.* [6] | 0.375×17×20 | 127.5 | single straight channel | separation of platelets from blood |
| Shu *et al.* [7] | 0.15×0.375×30 | 1.69 | single straight channel | particle enrichment |
| Ohlsson *et al.* [8] | 0.15×0.375×29 | 1.63 | single straight channel | separation of bacteria/blood cells |
| Present work | 0.6×0.6×292 | 105 | five straight channel sections connected by semicircular bends | material synthesis |

## 2. Ultrasonic microreactor

For the majority of the sonicated experiments the temperature rise was below 4℃, which remained stable even for long-term experiments due to the low power input of the designed reactor. As shown in Fig. S1, the temperature increases initially, and reaches a stable value after 10 min, with a maximum temperature increase of 6℃. For these experiments a T-junction with an inserted thermocouple was connected to the reactor outlet, and deionized water was used as flowing medium. It is worth noting that we did not apply any active cooling, and that the overall temperature increase could be lowered using e.g. a simple fan.

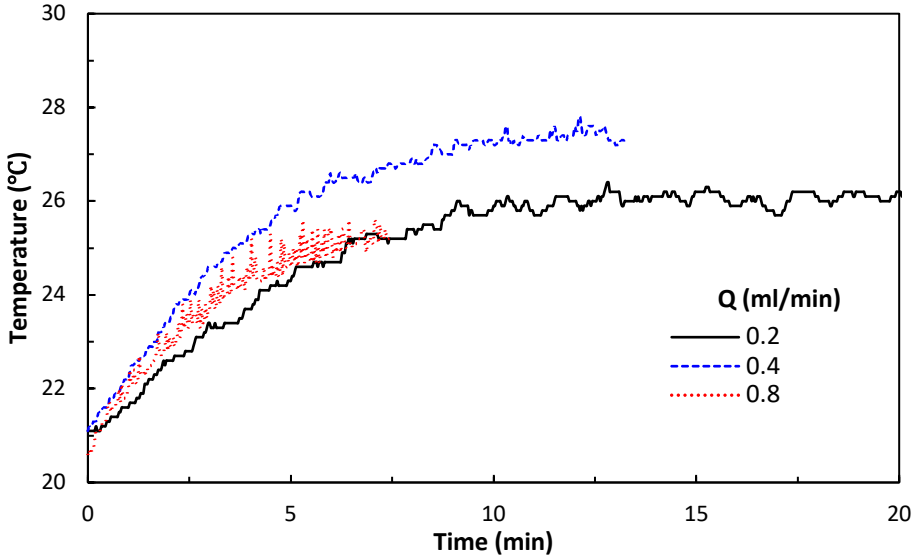


Fig. S1 Temperature rise of the ultrasonic reactor. The applied US voltage was 15 Vpp.

## 3. Inert particle focusing

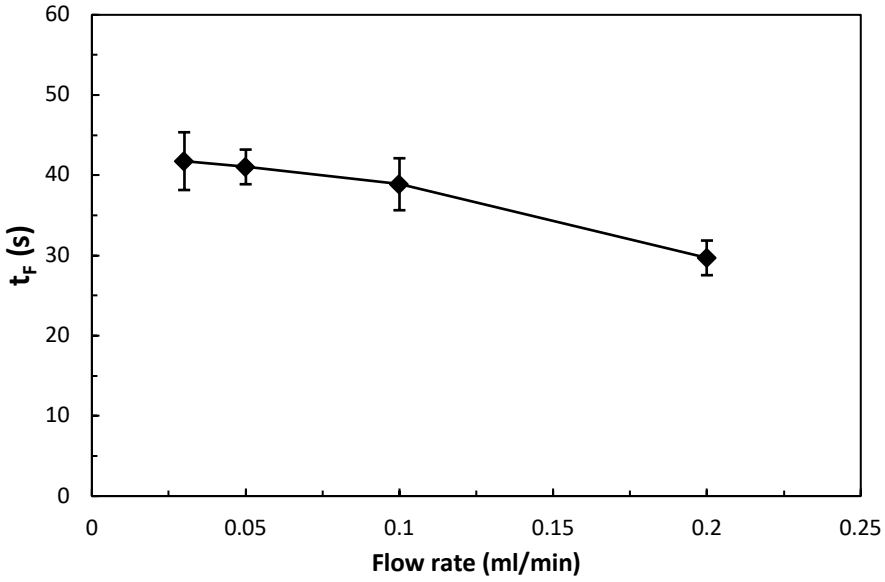


Fig. S2 Influence of flow rate on the focusing time $t_F$. The particle size is 12 μm and the applied voltage is 9.3 Vpp.

## 4. $CaCO_3$ synthesis

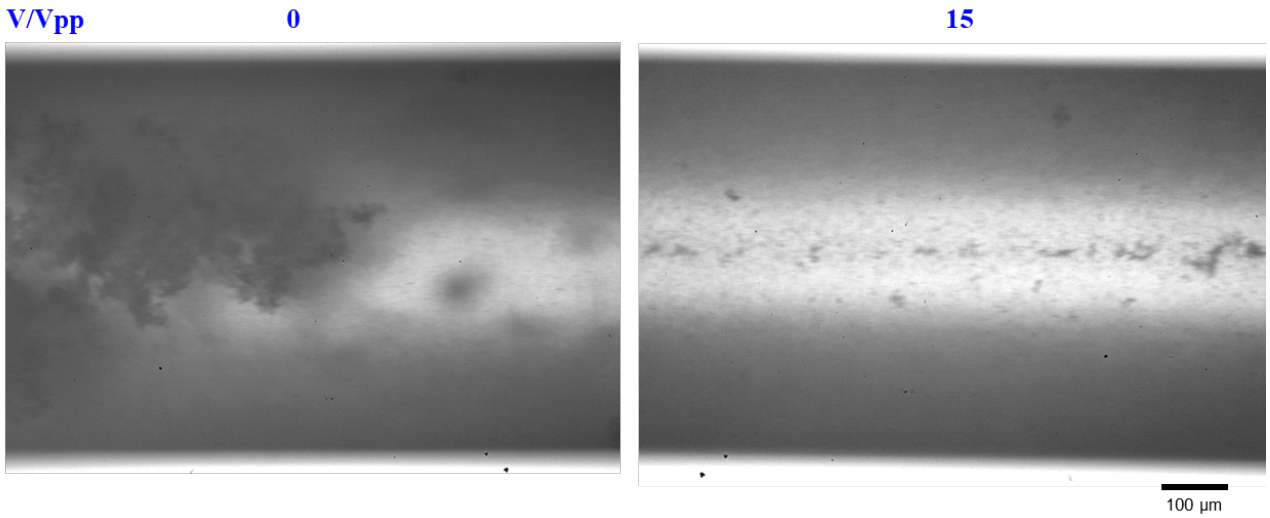


(a) (b)

Fig. S3 Images showing the distribution of the synthesized $CaCO_3$ particles in the channel without and with US. The reactant concentrations were 32 mM, and the total flow rate was 0.8 ml/min. The images are taken at location CH1 and the flow direction is from left to right.

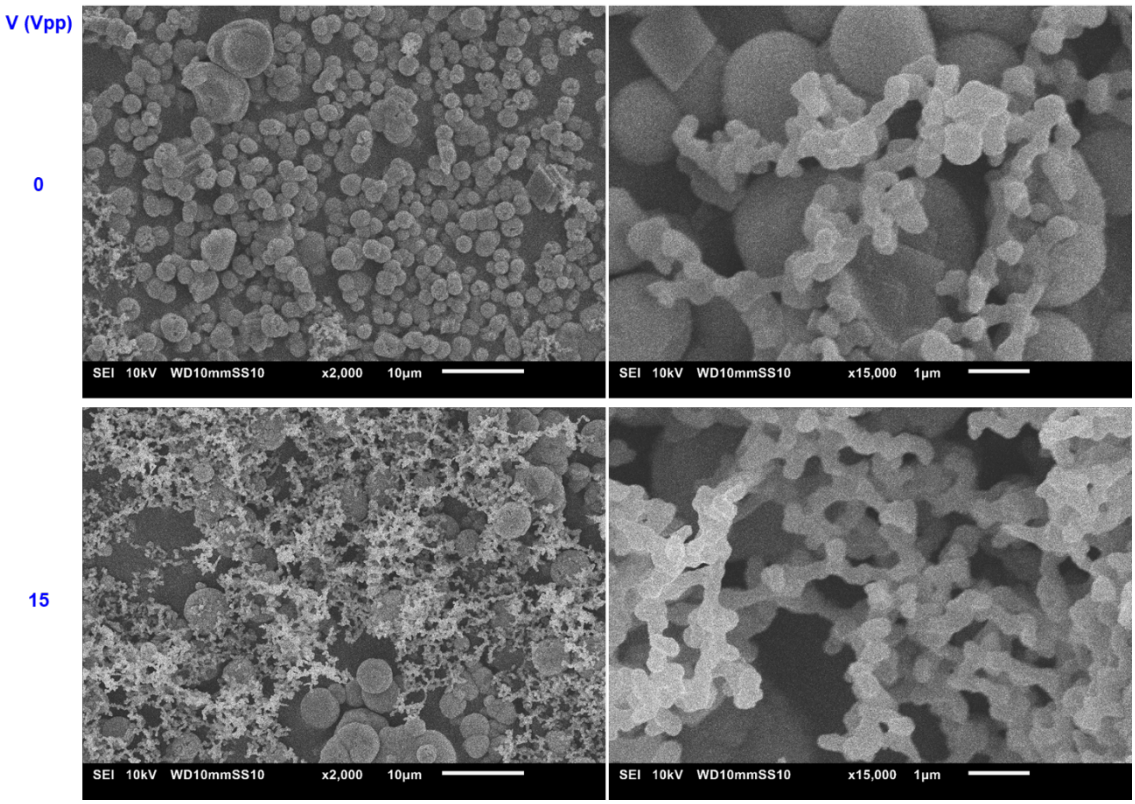


Fig. S4 SEM images of the synthesized $CaCO_3$ particles. The first row is without sonication and second row is for sonication with an applied US voltage of 15 Vpp. The reactant concentration was 12 mM, and the total flow rate was 0.8 ml/min. For SEM sampling, the outlet slurry was continuously filtered with a 0.22 um pore size nitrocellulose membrane on a Buckner funnel driven by a vacuum pump. The precipitate was then dried in an oven at 60 ℃ overnight. Before using the SEM (JEOL, JASM-6200), the powder was coated with a layer of Au/Pd allowing the sample to conduct electricity for the imaging process.

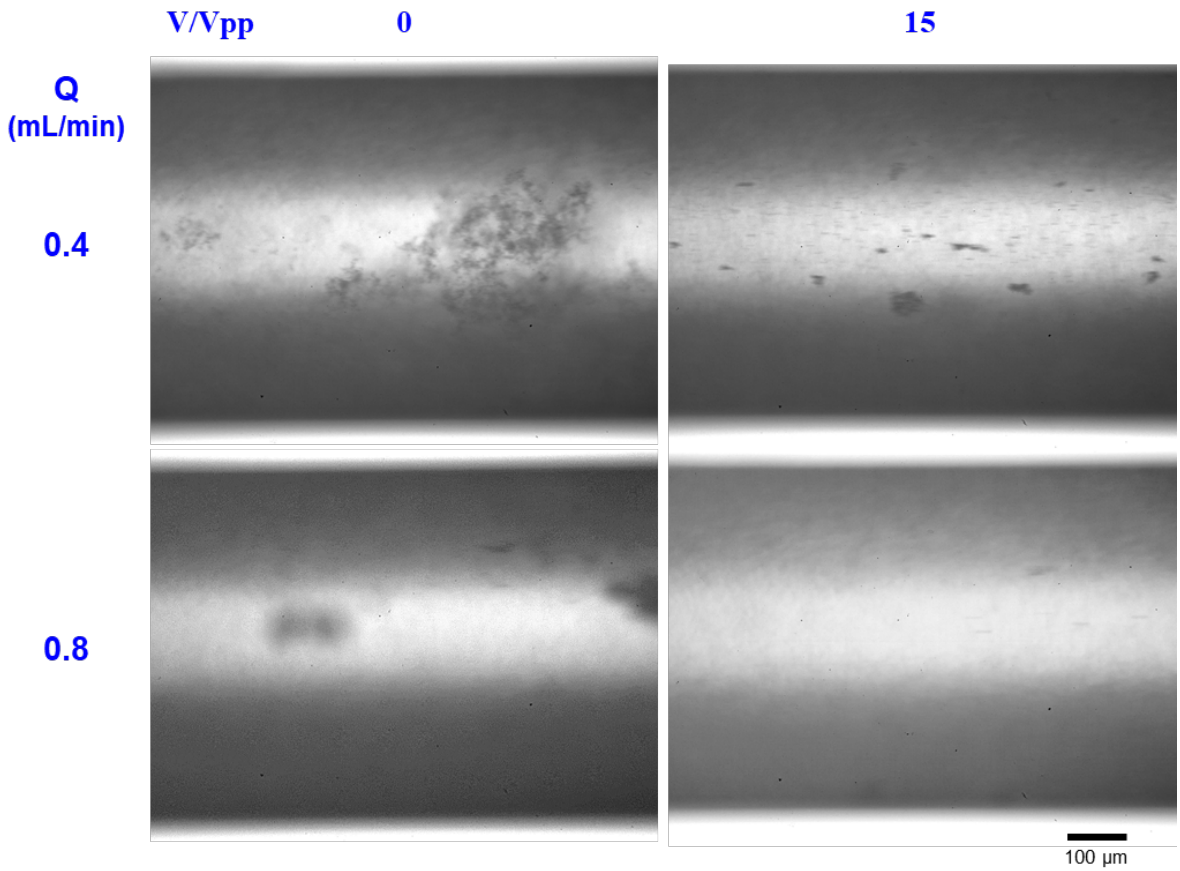


Fig. S5 Images showing the distribution of the synthesized $CaCO_3$ particles in the channel for different flow rates with and without US. Without US larger clusters and agglomerates of particles are observed. The reactant concentration was 12 mM, and the images were taken at location CH5. The flow direction is from left to right in all images.

## 5. Analysis of the acoustophoretic force on $CaCO_3$ and $BaSO_4$ particles

To compare the acoustophoretic force between $CaCO_3$/$BaSO_4$ and polystyrene particles, we adopt the radiation force equation for spherical particles in a planar standing wave [9,10]:

$$F = -\frac{\pi P_0^2 V \beta_0}{2\lambda}\phi(\beta,\rho)\sin\left(\frac{4\pi z}{\lambda}\right) \quad \text{(S1)}$$

with the contrast factor:

$$\phi(\beta,\rho) = \frac{5\rho_P - 2\rho_0}{2\rho_P + \rho_0} - \frac{\beta_P}{\beta_0} = 2.5 - \frac{4.5\rho_0}{2\rho_P + \rho_0} - \frac{\beta_P}{\beta_0} \quad \text{(S2)}$$

where $V$, $\rho_p$ and $\beta_p$ are the volume, density and compressibility of the spherical particle. $\rho_0$ and $\beta_0$ are the density and compressibility of the liquid (water: $\rho_0$=1 g/cm$^3$, $\beta_0$=45.6·10$^{-11}$ Pa$^{-1}$). $P_0$ and $\lambda$ are the sound pressure amplitude and wavelength. For particles of identical size, using the same solvent and the same acoustic condition, the strength of the radiation force changes linearly with the contrast factor. As shown in Eq. S2, the higher the density and the lower the compressibility the larger is the contrast factor, and the properties of $CaCO_3$, $BaSO_4$ and polystyrene are listed in Table S2. Due to the higher density and lower compressibility of $CaCO_3$, the contrast factor for $CaCO_3$ particles is 5.4 times larger than that for polystyrene. Therefore, the acoustophoretic force on $CaCO_3$ particles is 5.4 times stronger than that for polystyrene particles of the same size and in the same acoustic field. Similarly, for $BaSO_4$ the acoustophoretic force increases by a factor of 6.1 compared with the force acting on polystyrene particles, but only by a factor of 1.1 compared with $CaCO_3$.

Table S2 Properties of polystyrene, $CaCO_3$ and $BaSO_4$ particles

| Material | Density g/cm$^3$ | Compressibility 10$^{-11}$ Pa$^{-1}$ | Contrast factor |
|---|---|---|---|
| Polystyrene | 1.05 | 28.6 | 0.328 |
| $CaCO_3$ | 2.71 | 1.02 | 1.78 |
| $BaSO_4$ | 4.5 | 2.0 | 2.01 |

## References


[1] A. Neild, S. Oberti and J. Dual, Sensors and Actuators B, 2007, 121, 452–461.

[2] E. J. Fong, A. C. Johnston, T. Notton, S.-Y. Jung, K. A. Rose, L. S. Weinberger and M. Shusteff, Analyst, 2014, 139, 1192-1200.

[3] M. Antfolk, P. B. Muller, P. Augustsson, H. Bruus and T. Laurell, Lab Chip, 2014, 14, 2791–2799.

[4] M. Antfolk, C. Antfolk, H. Lilja, T. Laurell and P. Augustsson, Lab Chip, 2015, 15, 2102–2109.

[5] L. Gao, C. W. Shields IV, L. M. Johnson, S. W. Graves, B. B. Yellen and G. P. López, Biomicrofluidics, 2015, 9, 014105.

[6] Y. Chen, M. Wu, L. Ren, J. Liu, P. H. Whitley, L. Wang and T. J. Huang, Lab Chip, 2016, 16, 3466 –3472.

[7] X. Shu, H. Liu, Y. Zhu, B.Cai, Y. Jin, Y. Wei, F. Zhou, W. Liu and S. Guo, Microfluid Nanofluid, 2018, 22, 32.

[8] P. Ohlsson, K. Petersson, P. Augustsson and T. Laurell Scientific Reports, 2018, 8, 9156.

[9] L. A. Kuznetsova and W. T. Coakley, Biosens. Bioelectron., 2007, 22, 1567-1577.

[10] H. Bruus, Lab Chip, 2012, 12, 1578–1586.